Force Adaptive Hot-Wire Cutting

Integrated Design, Simulation, and Fabrication of Double-Curved Surface Geometries

Romana Rust, Fabio Gramazio, and Matthias Kohler

R. Rust, F. Gramazio, M. Kohler
Gramazio Kohler Research, ETH Zurich, Switzerland
rust@arch.ethz.ch
gramazio@arch.ethz.ch
kohler@arch.ethz.ch

S. Adriaenssens, F. Gramazio, M. Kohler, A. Menges, M. Pauly (eds.): Advances in Architectural Geometry 2016
 DOI 10.3218/3778-4_20, ISBN 978-3-7281-3778-4
http://vdf.ch/advances-in-architectural-geometry-2016.html

Abstract

This paper discusses a robotic cutting technique – Spatial Wire Cutting (SWC) – performed by the coordinated movement of two six-axis robotic arms which control the curvature of a hot-wire adopting itself against the resistance of the processed material. By escaping from the linearity of the cutting medium, combined with an integrated approach towards computational design, simulation and automated fabrication, this technique fosters the efficient manufacturing of double-curved surface objects by single cutting procedures and significantly expands the set of possible hot-wire cutting geometries. This paper presents a custom fabrication-informed computational design and simulation framework. It also outlines comparative analytical studies between digitally created SWC objects and their physically fabricated counterparts. Finally, it concludes with the architectural potentials of the discussed technique.

Keywords:
computational design, digital fabrication, hot-wire cutting,
feedback-based automated manufacturing, multi-robot control,
dynamic simulation

S. Adriaenssens, F. Gramazio, M. Kohler, A. Menges, M. Pauly (eds.): Advances in Architectural Geometry 2016
 DOI 10.3218/3778-4_20, ISBN 978-3-7281-3778-4
http://vdf.ch/advances-in-architectural-geometry-2016.html

1. Introduction and Background

Recent technological advances have fostered the relationship between digital design and fabrication of architectural freeform shapes, opening a cross-fertilizing field from which various research directions are evolving. However, fabricating bespoke double-curved surfaces with commonly used fabrication techniques such as CNC-milling or 3D printing still comes at a high cost due to inefficient material use and time consumption (Schipper et al. 2014). The consequences are the simplification and post-rationalization of a specific design proposition. Digitally controlled cutting techniques, however, which have become very common in the larger fields of architecture, design and construction (Pigram & McGee 2011; Rippmann & Block 2011; McGee, Feringa & Søndergaard 2012), offer a fast, low-cost and material-efficient fabrication of non-standard volumetric elements for diverse applications (such as bespoke formwork components, prototype construction, etc.). These elements are created through the repeated movement of a cutting medium (e.g. hot-wire, steel cutting wire, hot-blade; Broek et al. 2002) through a synthetic material (e.g. expanded polystyrene) that melts the material just in advance of contact (thermal cutting). However, depending on the cutting medium, the range of geometries is limited. The project 'BladeRunner' (GXN 2016) is one of the most recent approaches, in which a hot-blade is dynamically bent to cut "surfaces swept out by continuously varying families of planar Euler elastica" (Søndergaard, et al. 2016), that reduces the geometrical restrictions.

The research presented in this paper focuses on Spatial Wire Cutting (SWC), a novel cutting technique performed by two six-axis lightweight robotic arms connected through a single hot-wire, which is attached to their end-effectors (see Fig. 1). Contrary to the above-mentioned approaches, it operates in transition states between thermal cutting and thermo-mechanical cutting to utilize the forces opposite to the moving direction to manipulate the hot-wire, which takes up the form of a curve. This curve is controlled by the robot's coordinated movement and is constantly altered throughout the procedure. Hence, this technique allows to significantly expand the set of possible hot-wire cutting geometries to certain double-curved surfaces, in particular sweep surfaces, which can be defined by the motion of a changing profile curve along two trajectory curves.

To efficiently control this multi-robotic cutting process, an advanced robotic control system is developed that monitors occurring forces during the manufacturing process and adapts the velocity of the cooperating arms accordingly. The dynamic change of these forces throughout the whole cutting procedure determine the absolute geometry of the surface being cut. To design those artefacts, it is crucial to predict the physical behaviour, as an evolving interplay between velocity, heat input, and reaction forces. As such, the project proposes an integral approach towards adaptive fabrication, design and simulation.

S. Adriaenssens, F. Gramazio, M. Kohler, A. Menges, M. Pauly (eds.): Advances in Architectural Geometry 2016
 DOI 10.3218/3778-4_20, ISBN 978-3-7281-3778-4
http://vdf.ch/advances-in-architectural-geometry-2016.html

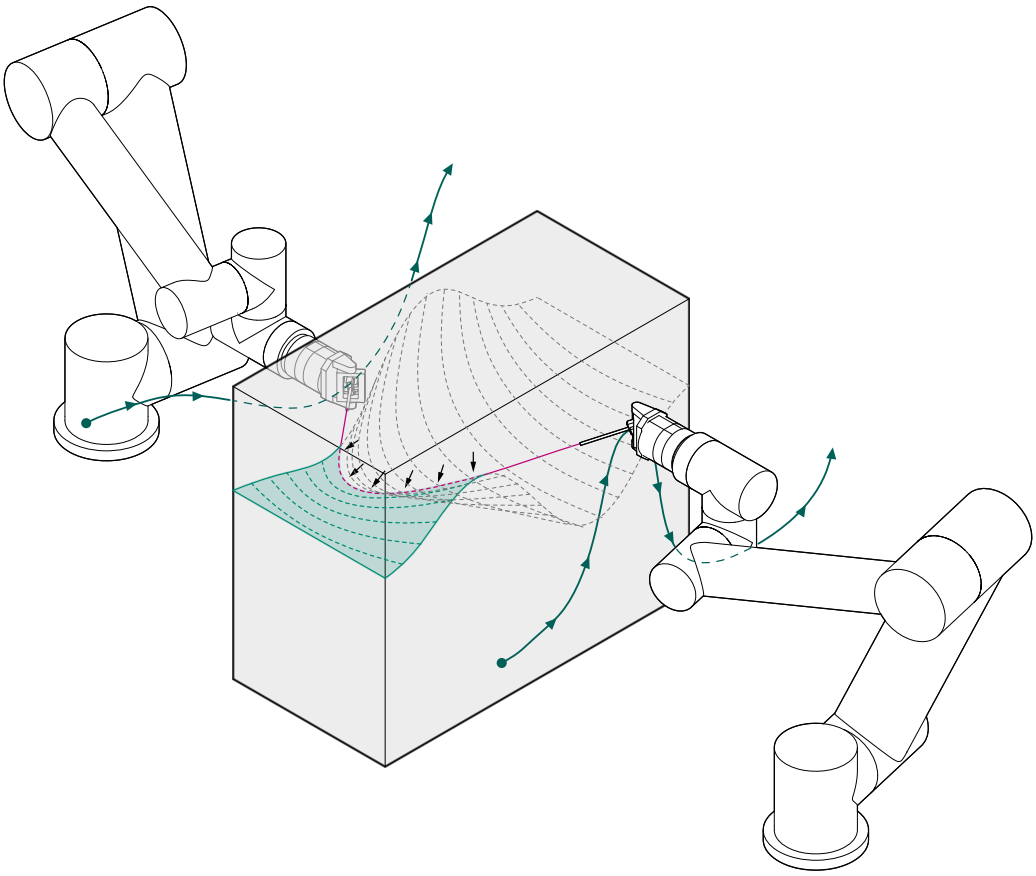

Figure 1. Illustration of the SWC cutting procedure, two robotic arms are moving on different path curves shaping the wire through material resistance (Rust et al. 2016).

In the next section (Section 2) the process variables and relationships that guide the procedure as well as their integration into the simulation framework, and further its embedding into the computational design setup, is presented. Section 3 outlines comparative studies of four surface objects, which have been simulated, fabricated, and 3D scanned. The analysis focusses on simulated and measured process data and a quantitative geometrical comparison. Section 4 discusses the results and addresses strategies to improve the combined simulation framework and fabrication system. The conclusions and outlook are summarized in Section 5.

S. Adriaenssens, F. Gramazio, M. Kohler, A. Menges, M. Pauly (eds.): Advances in Architectural Geometry 2016
 DOI 10.3218/3778-4_20, ISBN 978-3-7281-3778-4
http://vdf.ch/advances-in-architectural-geometry-2016.html

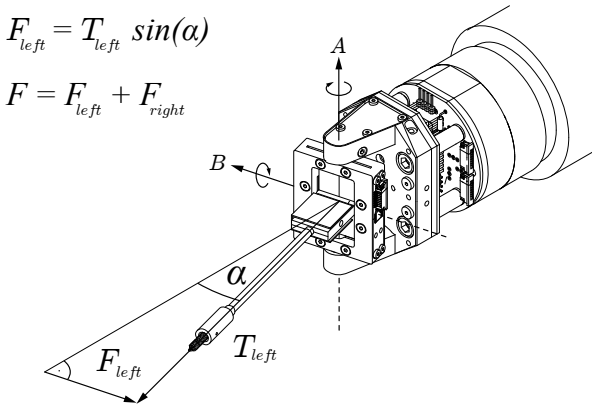

Figure 2. Cardan joint end-effector with axes (A, B), measuring angle α about axis A.

2. Fabrication-Informed Design and Simulation Framework

The shape of the wire and therefore the resulting surface is determined by forces acting on it throughout the cutting procedure. The magnitude of these forces as well as the force direction do not only vary along the cut, but also along the engaged wire in the foam. Their calculation is dependent on multiple factors such as the current speed, the heat input, the actual wire shape and the material properties of both the polystyrene and the hot-wire. In order to efficiently control the procedure and predict the resulting geometry, a digital model of the physical process has to be developed.

2.1 Process Variables

To identify the relationships between the most influential variables, such as heat input Q_1 [W/m], speed v [m/s], and resulting cutting force, a first series of cutting tests was performed. According to Ahn, Lee, and Yang (2003), Q_1 and v can be considered together as the effective heat input Q_{eff} [J/m^2] ($=Q_1/v$). In these tests the tension force T was recorded in steady state conditions[1], in which it levels off (Brooks 2009, 91). Additionally, the deflection[2] of the wire about the mounting points was logged (using a custom Cardan joint tool head with magnetic encoder sensors and a force sensor in the centre of the axes, see Figure 2). Thus, it was possible not only to map the tension force according to a given Q_{eff} in an exponential model (Bain 2011, 176–78), but also the resultant of all forces acting perpendicular onto the wire (see Fig. 4). The coefficients (a, b, c, resp. $\bar{a}$, $\bar{b}$) were found by model fitting and are material dependent (properties of polystyrene and hot-wire[3]).

S. Adriaenssens, F. Gramazio, M. Kohler, A. Menges, M. Pauly (eds.): Advances in Architectural Geometry 2016

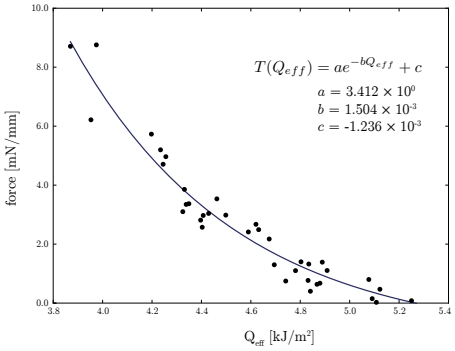

Figure 3. Model of relationship between Q_{eff} and tension force T in the steady state per unit of engaged wire length (Rust et al. 2016).

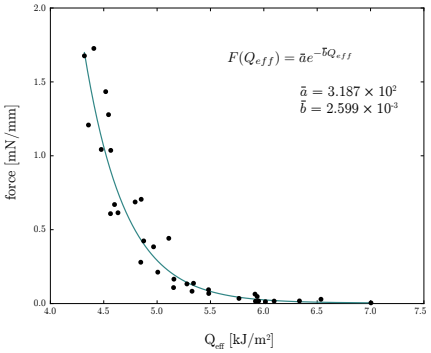

Figure 4. Model of relationship between Q_{eff} and material force F in the steady state per unit of engaged wire length.

(1)

$$T(Q_{eff}) = a\, e^{-b\, Q_{eff}} + c$$

(2)

$$F(Q_{eff}) = \bar{a}\, e^{-\bar{b} Q_{eff}}$$

2.2 Force Distribution

As the wire is exposed to variable forces, it deforms dependent on the magnitude, the direction, and the location of those forces, which ultimately influences the shape. For the fabrication process it is necessary to keep the wire always under a certain tension (based on empirical testing 2.0 N at each mounting point was defined as optimal value) to achieve a corresponding surface quality and, ultimately, to efficiently control the procedure.

To calculate the force distribution for a wire with a given shape of length s at a given moment t in time, it is discretized into $n-1$ segments and n nodes, with constant edge length l [mm] ($l = l_i$) between the nodes. Furthermore, for each node i the unit tangent vector $\hat{\mathbf{t}}_i$ is calculated. Assuming that the unit force direction $\hat{\mathbf{f}}_i$, the node speed v_i and heat input Q_i are known, the force vector $\mathbf{f}_i$ acting on one individual node i can be estimated as follows

(3)

$$\mathbf{f}_i = F(v_i, Q_l)\, l_i \left\| \hat{\mathbf{t}}_i \times \hat{\mathbf{f}}_i \right\| \hat{\mathbf{f}}_i,$$

S. Adriaenssens, F. Gramazio, M. Kohler, A. Menges, M. Pauly (eds.): Advances in Architectural Geometry 2016

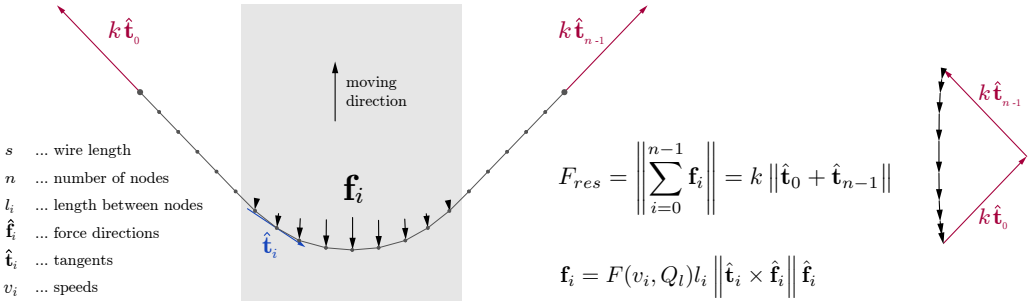

Figure 5. Force distribution on the nodes of the discretized wire.

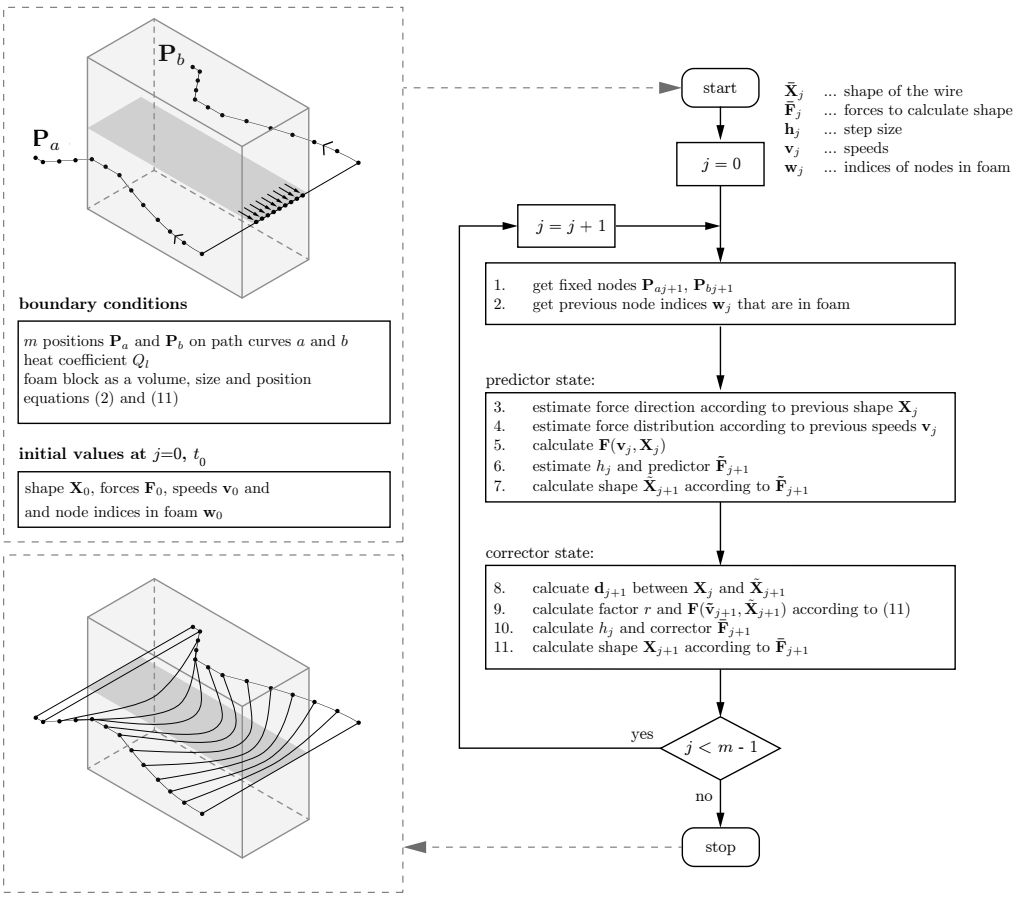

Figure 6. Schematic of the simulation algorithm.

S. Adriaenssens, F. Gramazio, M. Kohler, A. Menges, M. Pauly (eds.): Advances in Architectural Geometry 2016
 DOI 10.3218/3778-4_20, ISBN 978-3-7281-3778-4
http://vdf.ch/advances-in-architectural-geometry-2016.html

where $F(v_i, Q_i)$ is the force [N/mm] acting perpendicular to the engaged wire length according to equation (2) and $\| \hat{\mathbf{t}}_i \times \hat{\mathbf{f}}_i \|$ a ratio between 0 and 1 depending on the angle between $\mathbf{f}_i$ and the edge tangent $\hat{\mathbf{t}}_i$. Since the target tension force in the endpoints of the wire with tangents $\hat{\mathbf{t}}_0$ and $\hat{\mathbf{t}}_{n-1}$ is constrained to $k (= 2\,\mathrm{N})$, it is possible to calculate the resultant force F_{res}, which is the magnitude of the sum of all force vectors from equation (3):

(4)

$$F_{res} = \left\| \sum_{i=0}^{n-1} \mathbf{f}_i \right\| = k \| \hat{\mathbf{t}}_0 + \hat{\mathbf{t}}_{n-1} \|.$$

2.3 Shape Calculation

Since operating forces and shape are mutually dependent, it is assumed that the form of the wire at every moment t along the cutting trajectory is in an equilibrium state. Therefore, the force density method (Schek 1974) is applied to calculate its form. The two endpoints of the wire are set to fixed nodes with known positions $\mathbf{X}_f$, and according to applied forces $\bar{\mathbf{F}}\,[n \times 3]$, a vector $\mathbf{q}$ of force densities is sought, so that the length between each individual node matches the edge length l. The approach to find the target force densities $\mathbf{q}$ is performed iteratively (Veenendaal & Block, 2012): Starting with an estimated vector $\mathbf{q}_0$ the equation in (7) is solved for the unknown positions $\mathbf{x}_{u0}$:

(5)

$$\mathbf{D}_u = \mathbf{C}_u{}^T \mathbf{Q}_0 \, \mathbf{C}_u$$

(6)

$$\mathbf{D}_f = \mathbf{C}_u{}^T \mathbf{Q}_0 \, \mathbf{C}_f$$

(7)

$$\mathbf{D}_u \mathbf{X}_{u0} = \bar{\mathbf{F}}_u - \mathbf{D}_f \mathbf{X}_f$$

(8)

$$\mathbf{q}_{k+1} = \mathbf{Q}_k \, \mathbf{L}^{-1} \, \mathbf{p}_k$$

n_u, n_f …number for free (n – 2) and fixed (2) nodes

m …number of edges ($= n - 1$)

$\mathbf{C}_u[m \times n_u]$ …connectivity matrix of n – 2 free nodes

$\mathbf{C}_f[m \times n_f]$ …connectivity matrix of 2 fixed nodes

$\mathbf{X}_u[n_u \times 3], \mathbf{X}_f[n_f \times 3]$ …coordinate matrices of free and fixed nodes

$\mathbf{Q}_k$[m×m] …diagonal matrix of $\mathbf{q}_k$

$\mathbf{L}^{-1}$[m×m] …inverted diagonal matrix of the target edge lengths

According to $\mathbf{X}_0 (= [\mathbf{X}_{uo}, \mathbf{X}_f])$, the edge length vector $\mathbf{p}_k$ is calculated and the next force density vector $\mathbf{q}_{k+1}$ is estimated by (8), which is again inserted into equations (5) and (6) as diagonal matrix $\mathbf{Q}_{k+1}$, and the linear system in (7) is solved to calculate the new coordinates $\mathbf{X}_{k+1}$. This process is continued until a certain tolerance is reached and the sum of all edge lengths matches the wire length s.

S. Adriaenssens, F. Gramazio, M. Kohler, A. Menges, M. Pauly (eds.): Advances in Architectural Geometry 2016

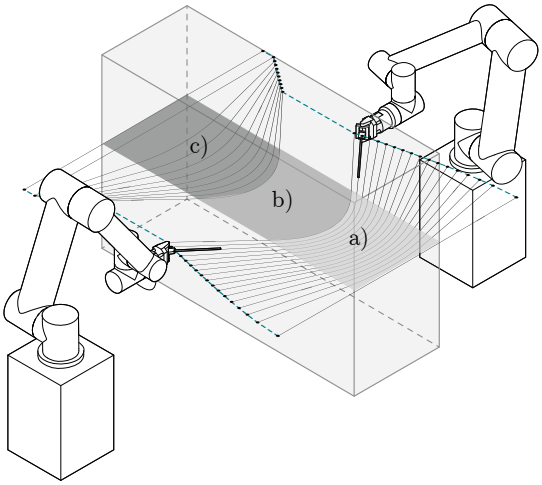

Figure 7. a) Entry, b) steady and c) exit phase.

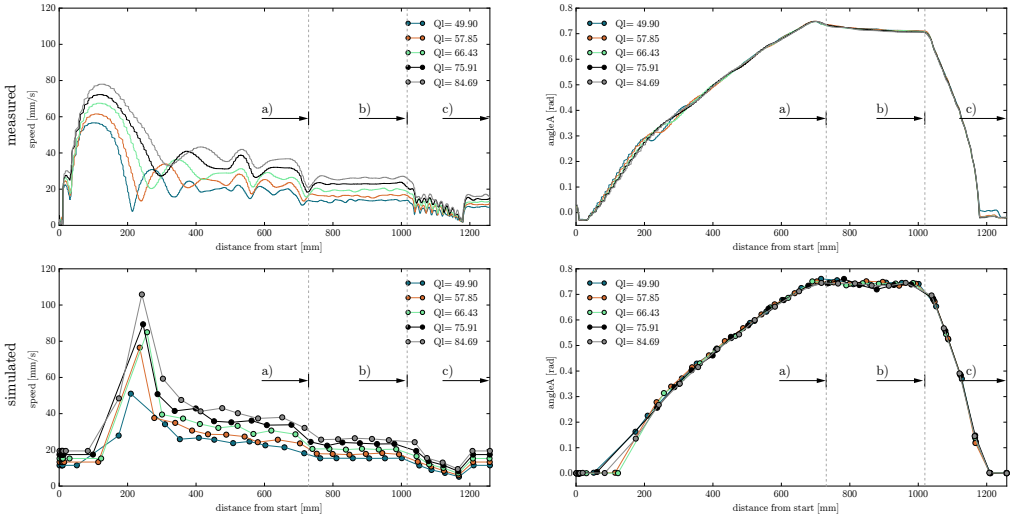

Figure 8. Measured and simulated process data (speed and angle) from five cutting tests with same path curves but different heat input.

S. Adriaenssens, F. Gramazio, M. Kohler, A. Menges, M. Pauly (eds.): Advances in Architectural Geometry 2016
 DOI 10.3218/3778-4_20, ISBN 978-3-7281-3778-4
http://vdf.ch/advances-in-architectural-geometry-2016.html

2.4 Simulation Model

The simulation model builds upon the simplified physical models as described in Sections 2.1 and 2.2. It is employed to predict the physical process to improve the control of the fabrication and to predict the resulting geometry.

The wire moving through the foam is a dynamic system. The boundary conditions are the path curves, respectively the synchronized positions on those curves, the size and position of the foam block as a volume, and a defined heat input. As mentioned in Section 2.1, the forces $\mathbf{F}$ (= matrix of all $\mathbf{f}_i$) in equation (4) are the steady-state forces that act at a certain moment. However, the shape is also dependent on the dynamic forces, and therefore the transient behaviour of the wire. The total forces $\bar{\mathbf{F}}$, used to compute the shape result from all forces that have occurred since the entry of the wire into the foam at t_0 to the current timestamp t_j. Therefore, a numerical integration is performed to integrate the forces over time.

The integration model for the simulation is a combination of the explicit Euler method with the trapezoidal rule and the predictor – corrector method (Heun's method). The steady-state forces $\mathbf{F}$ are a function of the shape and the speeds $\mathbf{v}$, $\mathbf{F}=\mathbf{F}(\mathbf{v}, \mathbf{X})$ acting at time t_j. The step size is denoted by h_j and initial forces $\bar{\mathbf{F}}_0=\mathbf{F}(t_0, \mathbf{X}_0)$. In the predictor step, starting from the current forces $\bar{\mathbf{F}}_j$, the next forces $\mathbf{F}_{j+1}$ are estimated with the Euler method:

(9)
$$\tilde{\mathbf{F}}_{j+1} = \bar{\mathbf{F}}_j + h_j \mathbf{F}\left(\mathbf{v}_j, \mathbf{X}_j\right),$$

from which the shape $\widetilde{\mathbf{X}}_{j+1}$ is calculated as described in Section 2.3. In the corrector step the initial guess is improved by using the trapezoidal rule:

(10)
$$\bar{\mathbf{F}}_{j+1} = \bar{\mathbf{F}}_j + \frac{1}{2} h_j \left(\mathbf{F}\left(\mathbf{v}_j, \mathbf{X}_j\right) + \mathbf{F}\left(\tilde{\mathbf{v}}_{j+1}, \widetilde{\mathbf{X}}_{j+1}\right)\right),$$

from which the shape $\widetilde{\mathbf{X}}_{j+1}$ is calculated. In each iteration step, the speed $\tilde{\mathrm{v}}_{ij+1}$ for one node i is estimated by $r\tilde{d}_{ij+1}$ (r factor, distances $\tilde{d}_{ij+1}=\|\mathbf{X}_{ij}-\mathbf{X}_{ij+1}\|$, $\mathbf{X}_{ij}$ position of node i at iteration step j). The secant method is applied to find the factor r and the root to the nonlinear equation (11), so that forces $\mathbf{F}(\tilde{\mathbf{v}}_{j+1}, \widetilde{\mathbf{X}}_{j+1})$ acting in the moment t_{j+1} comply equation (4).

(11)
$$g(r) = \left\|\sum_{i=0}^{n-1} F\left(r\tilde{d}_{ij+1}, Q_l\right) l_i \left\|\hat{\mathbf{t}}_{ij+1} \times \hat{\mathbf{f}}_{ij+1}\right\| \hat{\mathbf{f}}_{ij+1} \right\| - k \left\| \hat{\mathbf{t}}_{0j+1} + \hat{\mathbf{t}}_{n-1j+1} \right\| = 0.$$

S. Adriaenssens, F. Gramazio, M. Kohler, A. Menges, M. Pauly (eds.): Advances in Architectural Geometry 2016

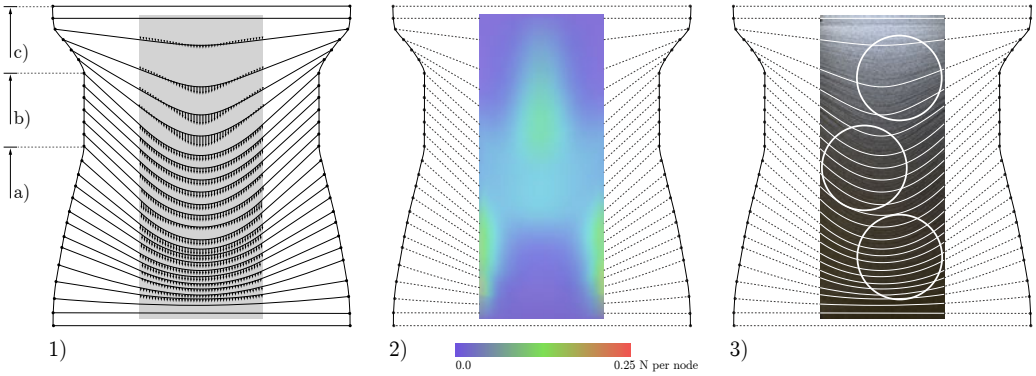

Figure 9. 1) Force vectors and curves from simulation, 2) force magnitudes coloured to visualize the differences and 3) overlay of surface picture with simulated curves.

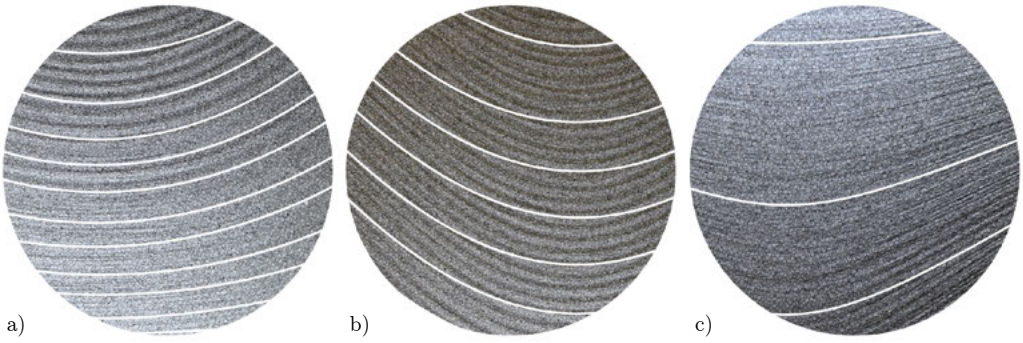

Figure 10. Details from the overlay between simulated curves and surface picture, from a) entry, b) steady and c) exit phases.

S. Adriaenssens, F. Gramazio, M. Kohler, A. Menges, M. Pauly (eds.): Advances in Architectural Geometry 2016

The step size h_j is calculated as the reciprocal value to the solution $r(h_j = d_{ij}/v_{ij})$, as the time between two iteration steps. After each iteration step, $\overline{\mathbf{F}}_{j+1}$ is downscaled, so that equation (4) is met and then multiplied by h_j; otherwise, the relation to the new force vectors $h_{j+1}y(\mathbf{v}_{j+1}, \mathbf{F}_{j+1})$ in the next iteration step wouldn't correspond.

2.5 Physical Validation

A series of cutting tests were performed a) to validate the force distribution model as stated in (3) and b) to verify if the force density method and the calculated wire shapes are coherent with the physical shape. Multiple cuts were performed with different foam block sizes (300, 400, and 500 mm in width and 1200 mm in length), different heat inputs (50–85 [W/m]) and different path curves. The robots' path curves were designed in such a way that all positions lay in the same horizontal plane but have different distances to each other, generating three phases that are of interest to the analysis, due to expected distinctive differences in the force distribution:

a) **Entry phase:** the wire starts straight but the wire's endpoints are continuously moving towards each other
b) **Steady phase:** the wire is in shape and the endpoints of the wire are moving parallel to each other
c) **Exit phase:** the endpoints of the wire move off each other

Results from the simulation are node positions of the discretized wire, from which NURBS curves are created, force vectors (magnitude and direction), estimated speeds and, according to the curves, also estimated angles of the wire's deflection about the mounting points. As such, it was possible to compare the measured speeds and measured angles with the simulated speeds and angles (see Figure 8). To uncover the wire's shape from the cut surface, it was illuminated from a sloped angle, the distortion of the picture taken was reversed, and the simulated curves were overlaid for comparison (see Figure 9).

The force magnitude colouring is an efficient analysis tool for the resulting surface and clearly exemplifies what happens inside the foam block. In the entry state, the outer nodes of the wire have to move faster than in the centre, producing higher forces in exit zones of the foam, while in the centre they reach zero force. Whereas in the steady zone, the force distribution is almost equal along the engaged wire and in the exit zone the reversed picture to the entry zone is visible, where the force in the exit zones are low, since the speed is lower than in the centre. Low forces can also be recognized on the physical surface, e.g. in the detail picture of (Figure 10, c): Low or zero force means thermal cutting, more material melted, producing more rills.

S. Adriaenssens, F. Gramazio, M. Kohler, A. Menges, M. Pauly (eds.): Advances in Architectural Geometry 2016
 DOI 10.3218/3778-4_20, ISBN 978-3-7281-3778-4
http://vdf.ch/advances-in-architectural-geometry-2016.html

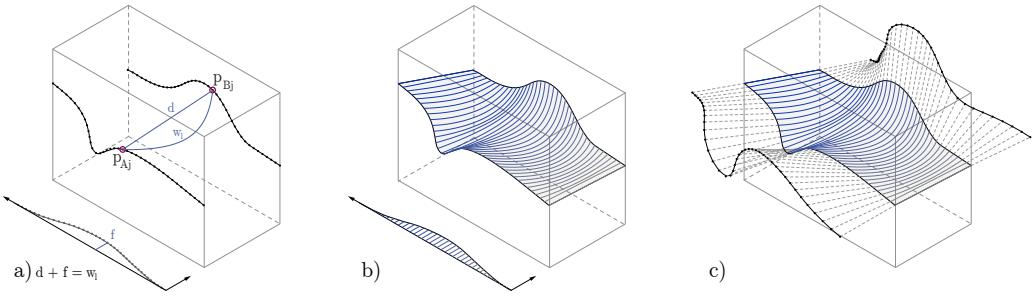

Figure 11. a) Edge curves, distribution of positions and wire length extension function, b) simulated curves and lofted surface thereof, c) extension of tangents to calculate path curves.

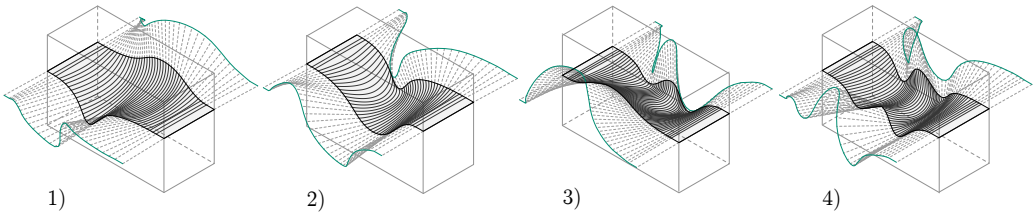

Figure 12. Surface design of different edge curve settings and robotic path curves.

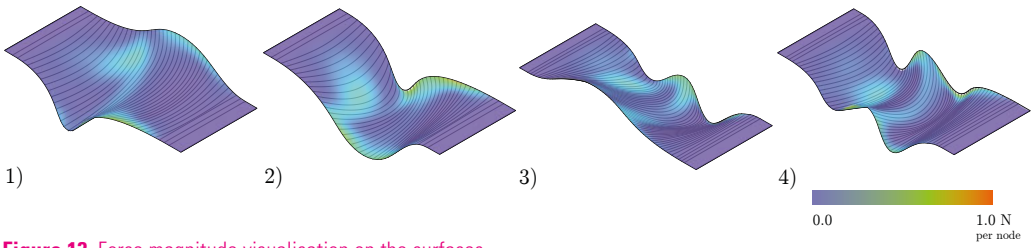

Figure 13. Force magnitude visualisation on the surfaces.

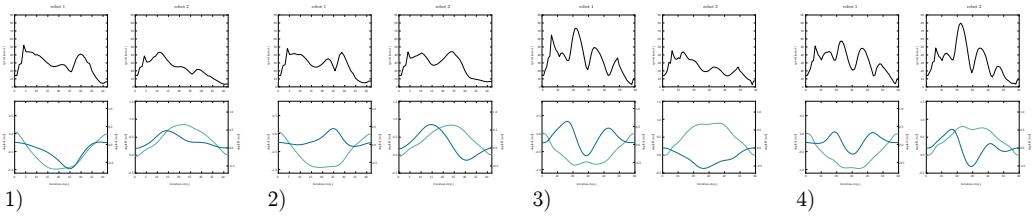

Figure 14. Estimated speed trajectories (black) and angles (blue, turquoise) for both robots.

S. Adriaenssens, F. Gramazio, M. Kohler, A. Menges, M. Pauly (eds.): Advances in Architectural Geometry 2016
 DOI 10.3218/3778-4_20, ISBN 978-3-7281-3778-4
http://vdf.ch/advances-in-architectural-geometry-2016.html

The results from the comparison of simulated process variables and measured process data of 20 cutting tests (as in Fig. 8) was very successful. Although the shape of the wire in the foam could just be visually compared, the simulated angle α, as the deviation of the wire about the mounting point had a normalized root-mean-square deviation (NRMSD) of just 0.06. The estimated speed trajectory also produced very good results and a similar NRMSD of 0.08 in the cutting tests. Thus, these tests proved physical coherency for the force distribution equation (3).

2.6 Computational Design

The procedure creates a specific set of double-curved surfaces. In order to design within this constrained design space, it is necessary to integrate design and simulation. The inputs for the simulation framework, as described in Section 2.4, are the path curves, respectively the positions on the curves and a defined heat input. But there is a counter-intuitive relationship between designing these curves and the resulting surface. Therefore, the initial simulation setup was altered to facilitate designing these surfaces: Instead of designing path curves, the edge curves of the surface on the foam block are designed, which are discretized into a number of points. Further, a function is created, that defines the additional length of wire to the distance between the points $\mathbf{P}_{aj}$ and $\mathbf{P}_{bj}$ (see Fig. 11, a).

As such, the simulation calculates the forces for nodes that are constantly in the foam, and the fixed nodes are the defined positions on the edge curves. However, since the length from one iteration step to the other changes, the nodes and their forces have to be redistributed. After all node positions have been calculated and NURBS curves have been created, a surface is lofted through the curves (see Fig. 11, b). To generate the path curves, a minimum distance to the foam block is defined and the simulated curves are extended at both ends in such a way that all curves have the same length (see Fig. 11, c).

This simulation framework was empirically tested and validated in a 2-week design and building workshop with students, which focussed on the development of novel façade typologies using bespoke cut polystyrene blocks as moulds. It was applied to design and generate a parametric model for the aggregation of robotically cut prototypes (Rust et al. 2016).

3. Comparative Studies

The potential of the cutting technique can clearly be expressed in cutting freeform shapes. Therefore, four different sample surfaces were designed, simulated, fabricated, and 3D scanned to provide an additional quantitative geometrical comparison between simulated surface and physical artefact.

S. Adriaenssens, F. Gramazio, M. Kohler, A. Menges, M. Pauly (eds.): Advances in Architectural Geometry 2016

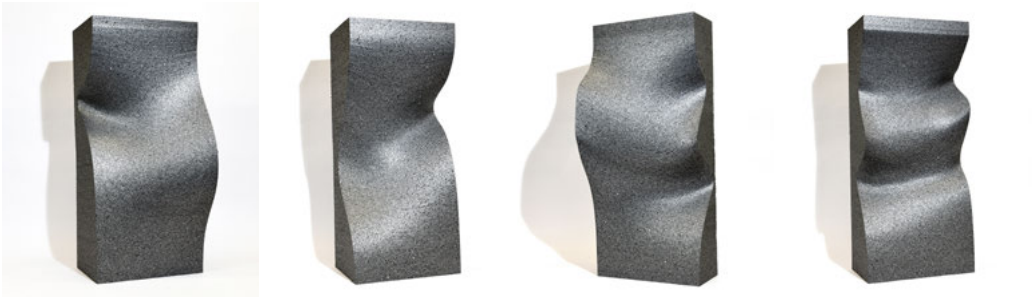

Figure 15. Fabricated objects 1) – 4), 400 x 900 mm (width x length).

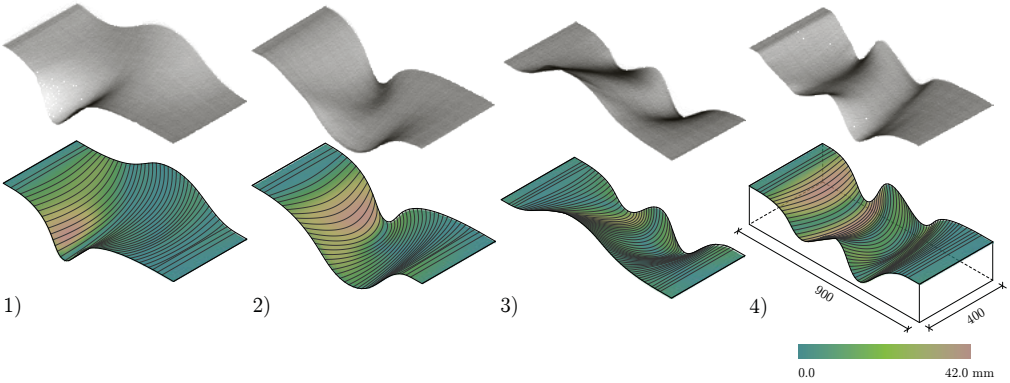

Figure 16. Simulated surfaces and point cloud data from the scanning process. The colours on the surface indicate the closest distance to the reconstructed mesh from the point cloud.

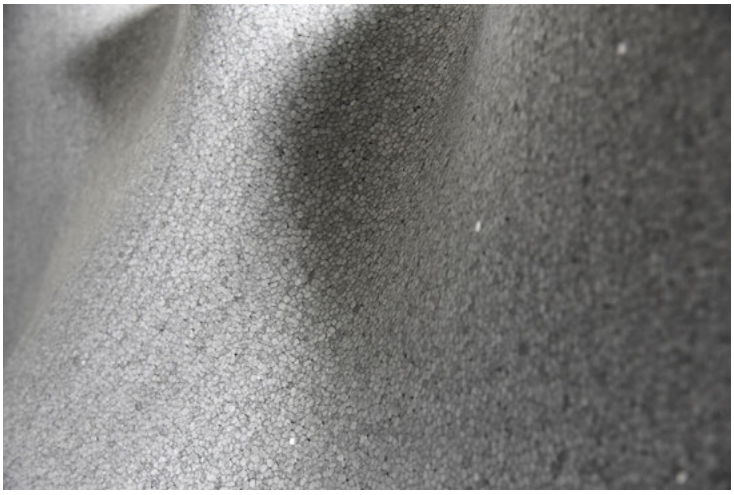

Figure 17. Surface detail.

S. Adriaenssens, F. Gramazio, M. Kohler, A. Menges, M. Pauly (eds.): Advances in Architectural Geometry 2016
 DOI 10.3218/3778-4_20, ISBN 978-3-7281-3778-4
http://vdf.ch/advances-in-architectural-geometry-2016.html

For the design of these surfaces, the edge curves and the wire length extension function, as input for the simulation, were designed in such a way to provide variability between moving directions and varying distances (see Figure 12). The estimated speed trajectories for the robots (see Fig. 14), calculated in the simulation, served as input for the fabrication procedure, which uses a combined feedback-feedforward control to tare the speed according to the force measurement about this estimated speed trajectory. After the fabrication the surfaces (see Fig. 15) were scanned and per surface an average over 1 million scan points were registered. From these point clouds a surface was reconstructed (Poisson surface reconstruction) and the closest distance to the simulated surface was calculated (see Fig. 16).

4. Results and Reflection

The comparison between simulated and measured process data, such as angles and speed trajectories, was similarly successful (speed: 0.14, angle α: 0.09, angle β: 0.06 NRMSD) as in Section 2.5. These results are clearly visible in the surface quality (see Fig. 17), proving a very good estimation of process variables and an efficient adaptive control. The maximum deviation in the geometrical comparison was 42 mm, which is still very high in terms of building tolerances. Areas of high deviation could be identified where the path curves show high curvature and at later moments in the procedure where deviations accumulate.

The simulation model is a simplification and an abstraction to the physical process. Factors that have not been integrated may have affected an accurate result. Amongst others, for example, the material force model (see Fig. 4) estimates the force under steady-state conditions, but actually the temperature of the wire is changing and constantly in transition states. These factors were assumed to have negligible influence, but small inaccuracies sum up along the process. Although the developed computational simulation framework cannot predict the resulting physical surface with absolute precision, the results are visually identical, and therefore it can be employed for digital design explorations that are coherent with their fabrication.

5. Conclusion and Outlook

A fabrication-informed design and simulation framework was presented and physically evaluated. It was demonstrated that the project's combined design and fabrication methodology allows for the efficient fabrication of unique and differentiated double-curved surface geometries, which brings forward a new geometric capability to existing hot-wire cutting techniques. The particular set

S. Adriaenssens, F. Gramazio, M. Kohler, A. Menges, M. Pauly (eds.): Advances in Architectural Geometry 2016
 DOI 10.3218/3778-4_20, ISBN 978-3-7281-3778-4
http://vdf.ch/advances-in-architectural-geometry-2016.html

of geometries imposes a constrained design space, which allows to reveal the specific tectonics of the process.

A coherency between digital and physical model was established. A further topic of research is to investigate methods to make these two models complementary, which is already partly achieved by correcting the estimated speed trajectory according to the force measurements. Thus, strategies to overcome the physical tolerances could either be the improvement of the simulation by integrating more physical behaviour or the improvement of the adaptive fabrication control to not only regulate the speed, but also to dynamically adjust the path curves to fulfil the desired geometric target. This opens up the question to which extent a process needs to be modelled in advance to be able to efficiently control it, which means either adapting the digital model to the physical process control, vice versa, or even both. Material and process-informed design methods are inherently soft design methods. They do not necessarily describe exact geometry but the constraints and rules that create geometry. A subject of further research, which relates to the question above, will be the investigation of such a soft control in respect to architectural design.

Endnotes

1 Steady-state conditions are reached at constant speed when the temperature and the cutting force level off.

2 In these tests the deflection, respectively the angle α, was kept below 10 degrees to mainly induce perpendicular forces on the wire.

3 The described experiments were performed with the foam swissporLAMBDA Vento (density: 15 kg/m^3) and the material for the hot-wire was Kanthal A with a diameter of 0.15 mm.

4 Since the measured data was oscillating in the beginning of the entry phase, the investigated phase was shifted thereafter. RMSD represents the sample standard deviation of the differences between the simulated values and measured values. NRMSD is the normalized RMSD according to the range of the measured data (= maximum – minimum value).

Acknowledgements

This research is enabled by and funded through an Architecture & Technology PhD fellowship from the Institute of Technology in Architecture (ITA) of ETH Zurich. The authors thank their team, the Department of Architecture (D-ARCH) of ETH Zurich and swisspor AG. Furthermore, special thanks to Ryan Luke Johns for all the significant pre-work in first feasibility study of SWC and Florian Rist gave valuable advice and help in the development and realisation of the custom cardan joint end-effector. The authors would like to thank Diederik Veenendaal for suggesting equation (8) and proofreading Sections 2.1 to 2.4.

References

Ahn, D.G., S.H. Lee, and D.Y. Yang. 2003. "A Study on the Influence of the Sloped Cutting Angle on Kerfwidth and Part Quality in the Hotwire Cutting of EPS Foam for the VLM-s Rapid Prototyping Process." *International Journal of Machine Tools and Manufacture* 43, 14: 1447–464. doi: 10.1016/s0890-6955(03)00170-6

Bain, J. 2011. "Thermomechanical Hot Tool Cutting and Surface Quality in Robotic Foam Sculpting." PhD diss., University of Canterbury. Christchurch, New Zealand.

Broek, J. J., I. Horváth, B. De Smit, A. F. Lennings, Z. Rusák, and J. S.M. Vergeest. 2002. "Free-form Thick Layer Object Manufacturing Technology for Large-Sized Physical Models." *Automation in Construction* 11, 3: 335–47. doi: 10.1016/s0926-5805(00)00108-4

S. Adriaenssens, F. Gramazio, M. Kohler, A. Menges, M. Pauly (eds.): Advances in Architectural Geometry 2016
 DOI 10.3218/3778-4_20, ISBN 978-3-7281-3778-4
http://vdf.ch/advances-in-architectural-geometry-2016.html

Brooks, H. 2009. "Plastic Foam Cutting Mechanics for Rapid Prototyping and Manufacturing Purposes." PhD diss., University of Canterbury. Christchurch, New Zealand.

GXN. 2016. 3xn – BladeRunner. Accessed May 27 http://gxn.3xn.com/#/projects/by-name/213-bladerunner

McGee, W., J. Feringa, and A. Søndergaard. 2012. "Processes for an Architecture of Volume." Edited by S. Brell-Çokcan and J. Braumann. In *Rob/Arch 2012: Robotic Fabrication in Architecture, Art and Design*, 62–71. Austria, Vienna: Springer.

Pigram, D., and W. McGee. 2011. "Formation Embedded Design: A Methodology for the Integration of Fabrication Constraints into Architectural Design." In *Integration through Computation: Proceedings of the 31st Annual Conference of the Association for Computer Aided Design in Architecture (ACADIA)*, 122–31. ACADIA. Calgary/Banff, Canada: The University of Calgary.

Rippmann, M., and P. Block. 2011. "Digital Stereotomy: Voussoir Geometry for Freeform Masonry-Like Vaults Informed by Structural and Fabrication Constraints." In *Proceedings of the IABSE-IASS Symposium 2011*, London, UK.

Rust, R., D. Jenny, F. Gramazio, and M. Kohler. 2016. "Spatial Wire Cutting – Cooperative Robotic Cutting of Non-ruled Surface Geometries for Bespoke Building Components." Edited by S.-F. Chien, S. Choo, M. A. Schnabel, W. Nakapan, M. J. Kim, and S. Roudavski. In *Living Systems and Micro-Utopias: Towards Continuous Designing, Proceedings of the 21st International Conference on Computer-Aided Architectural Design Research in Asia (CAADRIA 2016)*, 529–38. Australia, Melbourne, 30 March–2 April.

Schek, H.-J. 1974. "The Force Density Method for Form Finding and Computation of General Networks." *Computer Methods in Applied Mechanics and Engineering* 3, 1: 115–34. doi: 10.1016/0045-7825(74)90045-0

Schipper, H.R., S. Grünewald, P. Eigenraam, P. Raghunath, and M.A.D. Kok. 2014. "Optimization of the Flexible Mould Process for the Production of Double-Curved Concrete Elements." Edited by H. Justnes. *Program and Book of Abstracts for the 1st Concrete Innovation Conference (CIC), Oslo*, June 11–13, 1988.

Søndergaard, A., J. Feringa, T. Nørbjerg, K. Steenstrup, D. Brander, J. Graversen, S. Markvorsen, A. Bærentzen, K. Petkov, J. Hattel, K. Clausen, K. Jensen, L. Knudsen, and J. Kortbek. 2016. "Robotic Hot-Blade Cutting – An Industrial Approach to Cost-Effective Production of Double Curved Concrete Structures." Edited by D. Reinhardt, R. Saunders and J. Burry. In *Robotic Fabrication in Architecture, Art and Design 2016*, 151–63. Sydney: Springer International Publishing.

Veenendaal, D., and P. Block. 2012. "An Overview and Comparison of Structural Form Finding Methods for General Networks." *International Journal of Solids and Structures* 49, 26: 3741–753. doi: 10.1016/j.ijsolstr.2012.08.008

S. Adriaenssens, F. Gramazio, M. Kohler, A. Menges, M. Pauly (eds.): Advances in Architectural Geometry 2016